Evaluation of a compact high power pulsed fiber laser source for laser-induced breakdown spectroscopy

Gravel, Jean-François; Doucet, François; Bouchard, Paul; Sabsabi, Mohamad

National Research Council Canada   Conseil national de recherches Canada

Canada

JAAS

PAPER

Evaluation of a compact high power pulsed fiber laser source for laser-induced breakdown spectroscopy

Jean-François Y. Gravel, François R. Doucet,* Paul Bouchard and Mohamad Sabsabi

The aim of the present work is to evaluate the potential of a fast growing laser technology, the fiber laser, in the field of laser-induced breakdown spectroscopy (LIBS). Many compact fiber lasers are now available, which produce a high quality beam and deliver sufficient energy to generate optically interesting plasmas for analytical purposes at very high repetition rates. This technology has not been yet seriously investigated for LIBS applications. We summarize here the main specifications and analytical performances of this laser source coupled to three different spectrometers for the analysis of aluminium samples. Limits of detection in the low µg g^{-1} range are calculated for magnesium, copper, manganese, silicon, iron and chromium. Using a compact spectrometer, a low limit of detection of 1.1 µg g^{-1} is obtained for magnesium in aluminium. Ablation craters produced on aluminium are also characterized. Finally, we briefly illustrate the possibilities of the fiber laser for the LIBS analysis of another matrix, calculating limits of detection that are below 20 µg g^{-1} for silver, iron and nickel in copper.

1. Introduction

Laser-induced breakdown spectroscopy, or LIBS, is an optical emission spectroscopy technique that involves laser-generated plasma which combines all the required processes for atomic spectrometry: sample vaporization, atomization and excitation simultaneously. Although LIBS fundamentals have been known for more than 40 years, interest in the technology prior to 1980 has been mainly centered on the basics of plasma formation. A few instruments based on LIBS have been developed, but they have not been widely used. In the last decade, however, there has been a renewed interest in the technique for a wide range of applications, including remote sensing and on-line monitoring of processes in hostile environments.[1,2] This is due in part to the unveiling of significant technological developments in the components (lasers, spectrometers, detectors) used in LIBS instruments as well as emerging needs to perform real time/on-site measurements under conditions where conventional techniques are difficult to deploy or simply cannot be applied.

Recently, fiber lasers have become one of the hottest topics in photonics as the technology has grown in robustness, reliability and peak power. The term fiber laser refers to lasers with an optical fiber as the active gain medium and is also related to doped fiber amplifiers commonly used in master oscillator power amplifier (MOPA) configuration systems.[3] In MOPA designs, various types of lasers can be used as the seed source for light

amplification (Q-switched solid state, fiber laser, laser diode, *etc.*). In fiber MOPA (sometimes called MOFA for fiber-amplifier), the amplification is performed with the help of a doped active fiber (*e.g.* glass doped with Nd^{3+}, Yb^{3+}, Er^{3+}, Tm^{3+}, Pr^{3+}, combination of Yb^{3+} and Er^{3+},…) which is pumped by another source at a shorter wavelength (*e.g.* telecom grade diode lasers). A schematic representation of a typical MOPA system is presented in Fig. 1. (For more information on the fiber laser please refer to ref. 4–10 since the literature is already very rich on the subject and because this is out of the scope of this paper.) The use of telecom grade diode lasers brings an outstanding level of robustness, since these diode lasers are designed for 25 years of continuous operation. Offering the advantage of optical fiber beam delivery, these lasers are being commercially adopted at a rate faster than any previous laser technology.[11] They are used for a high number of practical applications, ranging from marking, welding, cutting, to telecommunications, surgery and micromachining operations. However, despite the high number
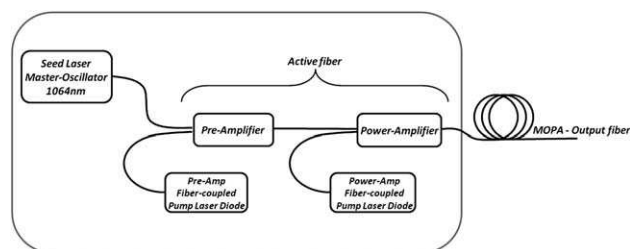
National Research Council Canada, Industrial Materials Institute, 75 de Mortagne Blvd, Boucherville, QC, Canada J4B 6Y4. E-mail: francois.doucet@cnrc-nrc.gc.ca

Fig. 1 Conceptual representation of a *master oscillator power amplifier*.

of interesting attributes which make fiber lasers very attractive for spectrochemical applications (high beam quality, low cost, robustness, broad range of wavelengths, energy delivery by fiber, user friendliness, high power efficiency rate, virtually mainte-nance free (>100 000 hours) *etc.*), their potential for quantitative LIBS analysis has not been extensively investigated yet.

Mainly because of their great marking potential, the concerns of most fiber laser users are more related to mechanical and physical properties of the ablated materials than to the analytical potential of the technology. However, there is no doubt that fiber lasers have evolved to a point where their characteristics in terms of energy per pulse (in the mJ range), beam quality (M^2 factor close to 1) and certainly its pulse width (from a few tens to hundreds of nanoseconds) have attained a level that is very interesting for LIBS applications. For these reasons, an evalua-tion of the analytical capabilities of the fiber laser is therefore very useful for LIBS users.

Another important aspect to consider is the compact size of the actually available fiber lasers. Great efforts have already been made to reduce the dimensions of the LIBS apparatus for the realization of portable instruments through the use of passively Q-switched microchips as laser sources. These microchips are compact, offer high quality beam and produce pulse energy in the range of a few tens of μJ. Their extremely short cavity length of several hundred micrometres produces pulse widths well below 1 ns and the passive Q-switch results in a repetition rate in the kHz range. A few papers have been published on the appli-cations of passively Q-switched microchips in LIBS.[12–17] Freedman *et al.*[12] and Lopez-Moreno *et al.*[13] investigated the applicability of microchip lasers in quantitative LIBS analyses of aluminium alloys and low-alloy steel, respectively. While in the first case the limits of detection (in the 0.05–0.14% range) were found to be poorer than required for a proper alloy classification, in the latter the limits of detection were lower than 100 μg g^{-1} for most of the chemical elements studied. More recently, Cristo-foretti *et al.*[14] evaluated a microchip laser with higher energy (80 μJ) for LIBS analysis of aluminium alloys and obtained limits of detection of the alloying elements which are competitive with a traditional LIBS system but still for some elements, higher by one order of magnitude. Another group examined the use of a microchip laser as the seed source in a custom MOPA system used for mines detection by LIBS.[18] And finally, Baudelet *et al.* recently published a paper on the use of a 2 μm thulium fiber laser (100 μJ per pulse with 200 ns pulse duration)[19] for LIBS applications. However, to our knowledge, the use of a compact commercial fiber laser emitting at 1064 nm for LIBS-based analysis of solids has not yet been studied.

In this paper, LIBS analysis capabilities of a compact fiber laser are evaluated and compared to those of traditional nano-second actively Q-switched flash lamp or diode pumped lasers. We used aluminium and copper alloys as reference for compar-ison because of the availability of reference data in our labora-tory, but also because it was commonly used in the LIBS literature. The laser unit used is described and a characterization of the craters obtained on an aluminium sample with this system is presented. The evaluation of the fiber laser as a LIBS source for quantitative analysis of various elements in aluminium and copper matrices is achieved using combinations of an echelle spectrometer/intensified CCD, of a benchtop Czerny–Turner spectrometer/intensified CCD, and of a low cost compact spec-trometer/non-intensified gated linear array detector. We high-light the analytical figure of merit by comparison to traditional LIBS setups using conventional flash lamp or diode pumped lasers, in the range of a few tens of mJ mainly. Finally, we discuss the advantages and drawbacks of the technology for LIBS applications in terms of ablation behaviour, sensitivity, energy delivery, repetition rate, analytical performances, standoff capabilities, *etc.*

2. Experimental

2.1. Laser and plasma generation components

A high power pulsed fiber laser model G3.0 SP-20P-HS-B-B-A-B (SPI Lasers, Southampton, UK) with an average power of 20 W, delivering light at 1064 ± 5 nm (Δλ full width at half maximum (FWHM) < 10 nm) is used for all the experiments. This pulsed MOPA laser is based on a laser diode as master oscillator combined to a dual-stage Yb GTWave™ amplifier. This patented technology, in opposition to traditional end or side pumping amplifier in dual-clad fibers,[20] uses multipoint pump injection. This is achieved by the use of a combined fiber composed of an active one and a pumping one properly placed in a common coating. It is claimed that this configuration allows uniform energy transfer between the pump and active fiber through all the length of the fibers' interaction thus minimizing "hot spots" and facilitating output–power scalability.[21] Combined to pulse-shaping technology, it can provide high peak powers for repeti-tion rates up to 500 kHz.

The laser may be operated at different energy outputs (*i.e.* 40 μJ up to 800 μJ per pulse) depending on the repetition rate selected. It can also be used in a continuous wave mode. Maximum energy output of 800 μJ per pulse is obtained at 25 kHz, but 32 pre-programmed "states" can be chosen from the laser unit. Each of them defines an electrical waveform impulse to the seed laser diode and a switching frequency. Any waveform can be used at any pulse repetition frequency but the maximum average power output stays constant (*i.e.* 20 W) for all frequen-cies over the switching one, thus giving less energy per pulse. In addition, the pulsed width can be adjusted from 15 ns up to 195 ns FWHM depending on the waveform and the repetition rate selected.

The high peak power generated by the laser pulse (*i.e.* 11 kW) is the main consideration for LIBS experiments. In order to meet the fluence and irradiance required to generate ablation and to produce a plasma, the waveform labelled "0", which produces the maximum output at 25 kHz delivering a pulse width of approximately 30 ns FWHM, has therefore been chosen. A typical temporal pulse shape of the laser output for waveform "0" at 25 kHz is compared to a traditional flash lamp pumped laser pulse in Fig. 2. It should be noted that the fiber laser was operated in extended hardware mode, a condition allowing enhanced flexibility for laser control (*i.e.* pulse on demand). The output of the fiber laser is coupled to a 7.0× beam expander model PT-P00318 (SPI Lasers), which produces a low divergence beam of 8.2 mm diameter. This beam is directed at normal incidence onto the target and focalised by a plano-convex lens of 75 mm focal length (PLCX-25.4-38.6-C-1064 CVI-Melles Griot,
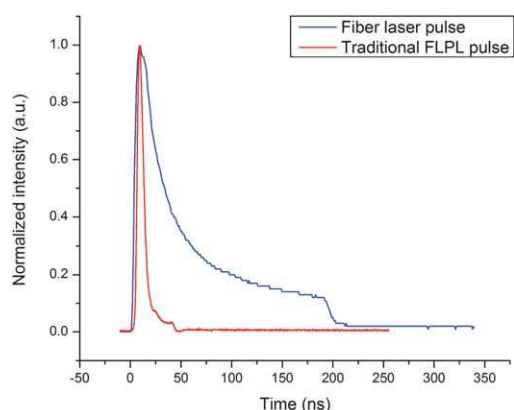
Fig. 2 Typical temporal energy distribution of a fiber laser generated pulse for waveform "0" at 25 kHz, 800 μJ pulse^{-1}, compared to a traditional Q-switch flash lamp pumped laser generated pulse.

New Mexico, USA). This combination of optics results in a focal spot of approximately 40 μm in diameter, leading to a fluence of 64 J cm^{-2} when using the laser at maximum energy. An experimental setup representation is shown in Fig. 3.

2.2. Light collection and detection

The light collection is achieved by the use of a corrected triplet lens (diam. = 25.4 mm, f = 90 mm, Edmund Optics, New Jersey, USA) located at 27 cm from the target and producing an image of the source onto the light collection fiber placed 14.5 cm behind. The axis of detection is 18° off the normal to the target surface. For our measurements, we evaluated three different commercial combinations of spectrometer/detector typically used in LIBS systems and LIBS laboratory setup. The first one is very compact and has a great potential in portable designs. The other two have high resolution but are more cumbersome.

2.2.1. Compact spectrometer. For the experiments done with the compact spectrometer, the collection fiber is a bundle of
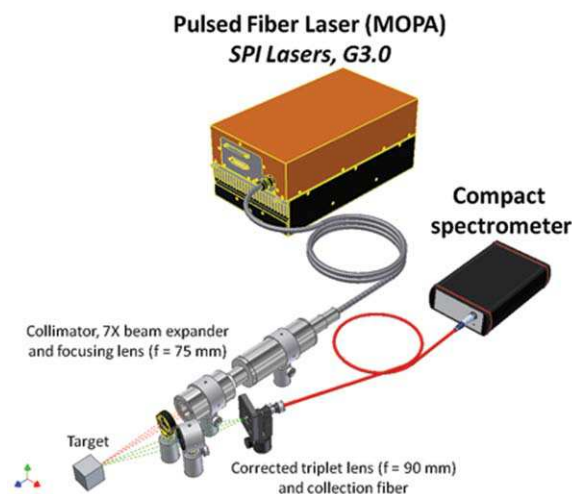

Fig. 3 Representation of the experimental setup with the compact spectrometer.

7×100 μm $\times$ 1 m in the configuration round (input) to line (output) (FCRL-7UV100-1, Avantes, Eerbeek, The Netherlands). The spectrometer is a 75 mm Czerny–Turner type UV/VIS spectrometer (AvaSpec 2048-USB2, grating: 600 lines mm^{-1} (UB), slit: 25 μm, Avantes) with a covered spectral range of approx. 220 nm to 775 nm using a gated linear CCD detector with 2048 elements. The chosen configuration leads to a linear dispersion of 19.35 nm mm^{-1} (*i.e.* 271 pm pixel^{-1} of 14 μm).

2.2.2. Benchtop spectrometer. We used a 0.34 m Czerny–Turner type spectrometer (model 340S, SPEX Industries Inc., Edison, NJ, USA) as a representative example for this category of commercial spectrometers. The collection fiber is a bundle of 25×100 μm $\times$ 10 m in the round to line configuration. The output of the fiber is directly used as the entrance slit of the spectrometer, which provides a 100 μm wide $\times$ 2.5 mm high illumination line at the spectrometer entrance. The grating used has 2400 lines mm^{-1}. The spectrometer is coupled to an anti-blooming intensified charge-coupled device (ICCD) detector (iStar DH-734-25F-03, Andor Technology, Belfast, Northern Ireland). Linear dispersion in that case is approximately 1.2 nm mm^{-1} (*i.e.* 23 pm pixel^{-1} of 25 μm).

2.2.3. Echelle spectrometer. The echelle spectrometer is a Mechelle 5000 (Andor Technology) coupled to an ICCD camera (iStar DH-734-18H-03, Andor Technology). The collection is achieved using a single 600 μm core diameter fiber. The entrance slit of the spectrometer is a square hole of 50 μm $\times$ 50 μm.

2.3. Synchronization and acquisition parameters

For our experiments, single shot acquisition has been considered as well as on-chip accumulation (for experiments involving an ICCD detector). In the single shot case, only the second pulse after the beginning of the fiber laser emission is considered; the first one being used to clean the surface. In the on-chip accumulation case, the accumulation of 15 shots is done at 25 kHz. A function generator (HP 3311A) was used as the main trigger to generate a 0.8 Hz to 30 Hz signal depending on the hardware limitations. This signal was then routed to a pulse/function generator (HP 8116A) where 25 kHz bursts are generated to trigger the fiber laser; these bursts of 2 or 15 pulses were supplied at a recurrence varying between 0.8 Hz and 30 Hz.

For single shot acquisition (2nd pulse only), the target was moved continuously using 3 motorized stages model UTM-100CC1HL (Newport, Irvine, CA, USA), as *X–Y–Z* displacement, controlled by a universal motion controller model ESP300 (Newport). Data acquisition was controlled using a custom application developed in LabView 7.1 (National Instruments, Austin, TX, USA) which synchronized the acquisition with the samples' translation in a manner to refresh the surface between each burst of two shots. In a first step, 150 single shot spectra were taken for each sample. Then, 10 "mean" spectra were generated, each of these being the average of 15 successive spectra from the initial 150 spectra collection. Statistics were done over the 10 spectra. For accumulation on-chip, bursts of 15 pulses were generated at the same spot before the sample was moved to renew the surface. In order to keep the analysis time and statistic similar to the single shot case, we made the

measurements at 10 different spots (15 shots × 10 positions ≈ 150 single shots). Statistics were done over those 10 spectra.

In all cases, a typical delay of 0.4 μs was used to eliminate the continuum of the plasma. The gate width was chosen large enough to cover the whole lifetime of the plasma with a typical value of 10 μs.

3. Results and discussion

3.1. Laser-produced crater characterization

The ablation performances of the fiber laser have been evaluated by means of optical coherence tomography (OCT) and scanning electron microscopy (SEM) measurements. Representations of OCT measurements are shown in Fig. 4a and 4b for a burst of 2 laser shots. It is possible to observe that a 2-pulse burst produces a crater depth of approximately 14 μm. Using the OCT results, the craters' depth and diameter have been evaluated for 10 craters with increasing number of shots, varying from 1 to 8 per crater. The averaged depth and width are reported in Fig. 5. The ablation rate seems to be linear from 1 to at least 8 pulses where approximately 7.7 μm pulse^{-1} is removed from an aluminium target.

Interestingly, the craters' aspect is significantly different from the ones produced by flash lamp pumped lasers (FLPLs) under similar irradiance conditions. The SEM images shown in Fig. 6 illustrate craters generated by bursts of 10 laser shots on aluminium. Obviously, the size of the crater produced by the fiber laser (Fig. 6a) is much smaller than the one generated by an FLPL at the same irradiance (Fig. 6b); i.e. 75 μm diameter for

Fig. 5 Craters' depth and diameter as a function of consecutive laser pulses per crater as determined from OCT measurements. Each value represents an average of 10 craters.

fiber laser vs. 240 μm diameter for FLPL. The crater depth per pulse is also significantly greater—7.7 μm pulse^{-1} compared to approx. 0.1 μm pulse^{-1} for FLPL. More importantly, minor visible traces of damage and recast material are present in the
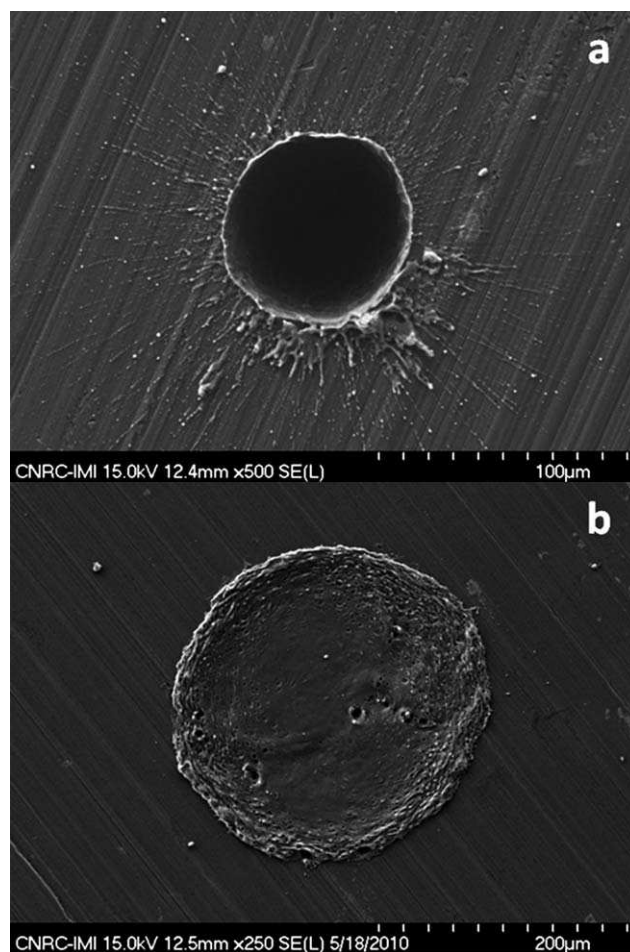
Fig. 6 SEM images of craters generated by (a) 10 consecutive laser shots at 25 kHz with the fiber laser and (b) 10 consecutive laser shots at 10 Hz with an FLPL at the same irradiance. Note the difference between scales.
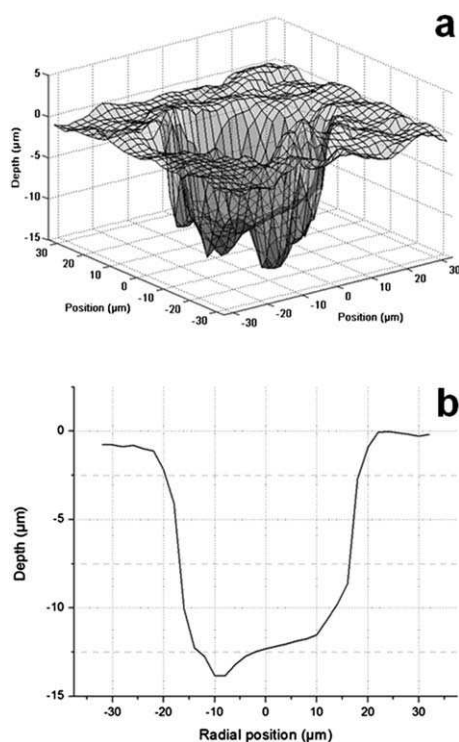

Fig. 4 (a) Typical 3D OCT crater image; (b) transversal representation of a crater based on OCT measurements. Fiber laser produced crater from a burst of 2 pulses in both cases.
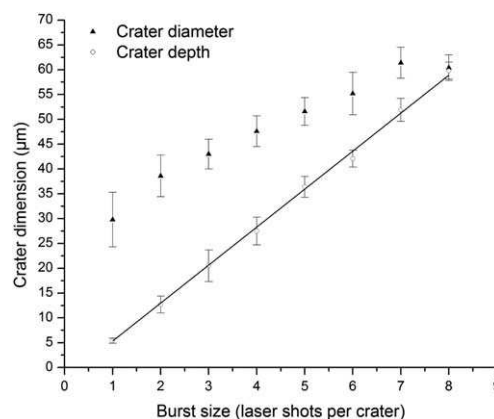
J. Anal. At. Spectrom.

This journal is © The Royal Society of Chemistry 2011

periphery of the fiber laser produced crater. The crater base also seems to be very uniform, which is of critical interest for a laser developed mainly for marking applications.

At first glance, one could attribute the high ablation rate to the very high repetition rate of the laser. This enhancement effect has effectively been illustrated by at least two groups for nanosecond lasers.[22,23] This behaviour was explained by heat accumulation on the target in the first case or by the presence of a hot rarefied gas region over the target—which reduces the shielding effect experienced by the subsequent pulses—in the second case. However, OCT comparison between craters produced by 10 subsequent laser shots at 25 kHz and craters produced from 10 shots at 1 Hz, with the same laser, shows no significant differences in craters' depths (5% deeper for 25 kHz burst) and only minor differences in the craters' diameters (15% larger for 25 kHz burst) (results not shown). Moreover, it is most probable that those minor differences are only related to the fact that the first laser pulse of each burst generated by the laser is slightly less energetic than the following ones (80% of the energy). In the case where 10 single pulses are produced independently, this diminution affects each of the 10 pulses, which might explain the small differences in the observed craters' depth and width. Experiments of Yamamoto et al. over the use of an acousto-optically Q-switched Nd:YLF laser operating at high frequency (6 kHz) with low energy and long pulses (150 ns) also support the hypothesis that for this kind of plasma, no inter-pulse effects are observable on the ablation or excitation process.[24]

The unusually high ablation rate observed here seems therefore to be related to the very high quality of the beam generated by the fiber laser ($M^2 = 1.6$–2.0) and to its relatively long pulse duration. Both characteristics also apply to the diffraction-limited nanosecond beam (25 ns) produced by copper vapour lasers (CVL), which are known to provide laser ablation features of exceptional quality.[25] One explanation for this might be related to the fact that these two characteristics affect the local irradiance at the target surface which influences the laser–plasma interaction mechanisms and therefore the amount of energy that reaches the target. It is known indeed that absorption of the laser energy can be related to various phenomena such as inverse Bremsstrahlung and laser-supported waves and that the importance of this energy absorption is a function of irradiance.[26–29] Bogaerts group's simulations in particular predict that the energy absorption within the plasma increases as a function of irradiance up to 80% for an irradiance value of 10^{10} W cm^{-2}.[29] Experimental work done by Cristoforetti et al. suggests that at a fixed fluence, laser ablation is more efficient for longer pulse width.[30] They also suggest that under a certain irradiance threshold (8–9×10^8 W cm^{-2}; which is slightly higher than the calculated irradiance for the fiber laser), the electron density within the plasma does not reach the critical value where avalanche photoionization and electron cascade responsible for strong pulse absorption normally occur. Shadowgraph experiments done by Gravel and Boudreau also showed that a strong energy coupling, leading to the initiation of laser-supported waves, is observed for irradiance values in the GW cm^{-2} range and higher.[31] They illustrate that the presence of "hot spot" zones in the beam's transverse energy distribution directly influences this threshold value. In the present case, one can suppose that the long pulse duration ($\sim$200 ns) combined to a moderate peak

irradiance (0.75 GW cm^{-2}) produced by the "hot spot free" fiber laser allows a good energy transfer to the solid target while keeping the absorption in the plasma to an acceptable level. We suppose that the irradiance at the target surface is below the threshold for laser-supported wave mechanism initiation, but specific shadowgraph or plasma imaging experiments would be needed to definitely state on that.

In addition to this impressive ablation behaviour, the high quality beam, combined to the large diameter output of the 7.0$\times$ beam expander, is relatively easy to focus on a small spot required to generate the high local peak irradiance ($\sim$0.75 GW cm^{-2} during first 30 ns, see Fig. 2) needed for LIBS experiments. In our setup, a standard 75 mm focal length plano-convex lens was used, allowing a good working distance and sufficient "LIBS depth of focus". We call "LIBS depth of focus" the z position range where the LIBS signal is independent of the working distance. In our case, it corresponds to approximately 800 μm. This tolerance to z position has to be considered when analysing rough unpolished surfaces.

3.2. Plasma characterization

Using the Boltzmann plot method described in ref. 32, with the assumption of local thermodynamic equilibrium and optical thinness of the plasma, the excitation temperature of the produced plasma was determined with a good repeatability up to
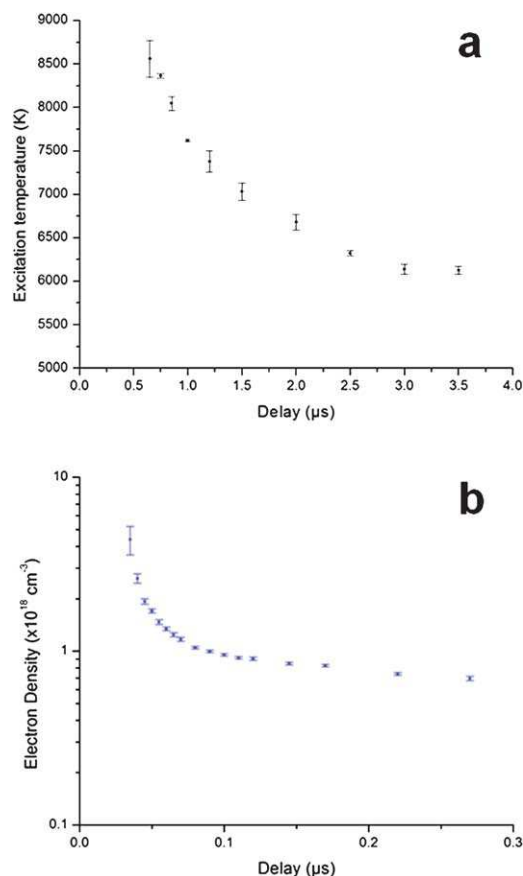

Fig. 7 Aluminium plasma (a) excitation temperature and (b) electron density as a function of time.

3.5 μs after the laser pulse (Fig. 7a). Beyond this delay, the emission of the iron lines used for the calculation became too weak to be measured with adequate precision. Moreover, the plasma cools down very rapidly and the total aluminium plasma emission lifetime is estimated at about 6–8 μs. This fast decay in temperature has previously been noticed for plasmas formed in similar conditions—irradiance and pulse length—and was attributed to their small size and high surface-to-volume ratio.[24]

We found indeed that the total plasma size was around 125–150 μm in diameter. This was done using a Spiricon SP620U camera with Beam Gage analysis software (Ophir-Spiricon, Logan, UT, USA) which allowed us to observe an axial image of the plasma produced by the collecting optics at the optical fiber position. The axial energy distribution was then Gaussian fitted and the diameter was determined at $1/e^2$. Considering that the magnification factor is equal to −0.25, it is clear that the whole image of the plasma (~35 μm) is easily coupled through any of the optical fibers used in those experiments.

The electron density of the laser-induced plasma was evaluated using the Stark broadening procedures described elsewhere (Fig. 7b).[32] The ionic line of aluminium at 281.6 nm was used to evaluate the plasma electron density; calculations lead to a value of approx. 7×10^{17} e⁻ cm⁻³, 0.3 μs after the laser pulse. The temporal density profile for delay values below 0.3 μs is presented in Fig. 7b. The electron density of this plasma is similar to what we found in a traditional FLPL generated plasma.[32] However, due to its tiny size, a very fast evolution is noticed.

3.3. Aluminium samples' analysis

Up to seven certified aluminium alloy samples were used for the preparation of each calibration curve. Depending on the linear range of the selected line, some high concentration points have been removed for the linear regression fit of some elements. None of the low concentration points have been discarded in any case. The difference between the peak maximum and the background level has been used without normalization to extract the information of every element line prior to building the calibration curves.

3.3.1. Echelle spectrometer.
Considering each laser-induced plasma as a short transient event, one could be interested in having the entire spectrum recorded at one time. The echelle type spectrometer allows achieving this with a very high resolution, and many LIBS applications took advantage of this

feature,[33–35] although it is sometimes accompanied by a decrease in light throughput. In our case, due to the size of the plasma, single shot plasma does not generate sufficient signal onto the detector. It was therefore necessary to sum and average the information over multiple laser shots for proper quantitative determination.

Using on-chip accumulation, very acceptable limits of detection (LODs) are obtained in aluminium with the echelle spectrometer (Table 1). The calculated LODs are interestingly comparable to the results obtained by Cristoforetti et al.[14] for aluminium analysis using an echelle type spectrometer and a compact spectrometer with a low energy diode pumped laser. In fact, all the LODs calculated in their work ranged within a factor of 0.5 to 2.5 from ours, with equivalent setups (except for Mn with the compact spectrometer where our detection limit is 15 times better). For the specific case of the echelle spectrometer, we can also compare to results obtained previously in ref. 36–38, where a lot more energy is used (i.e. 60 mJ pulse⁻¹, 70 mJ pulse⁻¹ and 300 mJ pulse⁻¹ respectively). Here, the LODs we found are higher by less than one order of magnitude for all elements except for Mg, where LODs ranged between a factor of 3 above and 3 below our detection limit. Considering the 800 μJ output of our laser, the results are impressive. The large ablated volume per pulse is without doubt responsible for this high relative detection sensitivity. In fact, more material is sampled from the target at each shot with the fiber laser compared to standard FLPL pulse (deeper crater and less melted-up volume) which may explain the great relative concentration sensitivity obtained despite the small produced plasma. In addition, the tailing in the temporal energy distribution of the pulses produced by the fiber laser may increase the LIBS signal. It has been demonstrated among others that pulse duration can affect the LIBS signal intensity and line shape.[30,39] More experiments would be necessary in order to confirm this possible contribution.

It is interesting to note that on-chip accumulation contributes to enhance the signal to noise ratio (S/N) in our experiments without influencing the experiment duration. Due to the high repetition rate of the laser (25 kHz), it is possible indeed to achieve the 15 shots accumulation on-chip within 600 μs by using the intensifier's fast gating capability, without affecting the integration time of the CCD. This allows one to get more signal faster, which is a non-negligible advantage considering that the maximum achievable rate with a traditional ICCD camera in the full image transfer mode—needed with an echelle spectrometer—is limited to approximately 0.8 Hz.

Table 1 LIBS limits of detection for Cr, Cu, Fe, Mg, Mn, and Si in an aluminium matrix for various spectrometers and acquisition methods using the compact fiber laser. No normalization is applied

Spectrometer	Echelle		Compact		Benchtop			
Acquisition method	On-chip accumulation		Single shot		Single shot		On-chip accumulation	
Element (line)	R^2	LOD/μg g⁻¹	R^2	LOD/μg g⁻¹	R^2	LOD/μg g⁻¹	R^2	LOD/μg g⁻¹
Cr (425.41 nm)	0.994	108 ± 4	0.996	10.8 ± 0.3	0.998	15.4 ± 0.3	1.000	12.1 ± 0.1
Cu (324.75 nm)	0.998	119 ± 5	0.999	6.5 ± 0.2	0.998	1.23 ± 0.05	0.996	3.1 ± 0.2
Fe (371.99 nm)	0.964	1300 ± 100	0.966	210 ± 20	0.980	51 ± 4	0.945	80 ± 10
Mg (285.21 nm)	0.970	9 ± 1	0.994	1.1 ± 0.1	0.970	0.75 ± 0.09	0.980	1.5 ± 0.1
Mn (403.07 nm)	0.924	70 ± 10	0.990	4.4 ± 0.3	0.983	7.8 ± 0.7	0.994	4.6 ± 0.2
Si (288.16 nm)	0.991	520 ± 30	0.997	82 ± 3	0.997	56 ± 2	0.999	80 ± 2

3.3.2. Compact spectrometer. Another kind of spectrometer, which is of growing interest, is the compact type, with an integrated linear CCD detector array. This detector has a relatively low noise level and can perform time-resolved measurements to eliminate the contribution of the continuum to the background. The high number of photons going through the system and the low dispersion of the spectrum (270 pm pixel^{-1}) allow obtaining very interesting LODs in aluminium with single shot acquisition, as we can see in Table 1. In fact, the LOD calculations show an improvement of approximately an order of magnitude for all the elements as compared to the echelle spectrometer in best conditions. Similar improvement was also reported by Cristoforetti *et al.*[14] by the use of a compact spectrometer.

In the particular case of aluminium analysis, or when the spectral background of the matrix is relatively simple, the compactness of the spectrometer does not affect the LIBS analysis because interference-free lines are easy to find. It even allows improving the analytical performances and the acquisition rate. Using those components with a lighter acquisition program would even allow us to attain several hundred Hz in acquisition rate for LIBS measurements. This advantage is noticeable as compared to the limited acquisition rate of 0.8 Hz for the echelle spectrometer and opens possibilities for fast 2D mapping of surfaces, as well as global concentration determination for inhomogeneous samples such as rocks or powdered materials. Actually, efforts are being devoted to the study of those aspects within our own laboratory.

3.3.3. Benchtop spectrometer. A benchtop Czerny–Turner spectrometer has also been used for comparison purposes. Slightly better limits of detection have been found for Cu, Fe, Mg and Si, but worst LODs have been achieved in the case of Mn and Cr when compared to the compact spectrometer (Table 1). The deterioration of the LOD in the case of Mn is probably related to the fact that the line considered for the calculation is the first of three very close lines that are unresolved in the case of the compact spectrometer. To minimize changes in parameters for the study, the light collection triplet is kept at the same location through all the experiments. This optimum position was determined for the compact spectrometer system collection fiber which is considerably smaller than the one used for the benchtop spectrometer. This, in fact, may contribute to deteriorate the LOD calculation for the benchtop spectrometer which could have tolerated in theory a larger magnification factor from bringing the collection triplet closer to the target, thus increasing the light collection solid angle.

3.4. Copper samples' analysis

Using the same parameters as for the aluminium analysis, we extended our tests to a copper matrix. Because the plasma is weaker and the spectral background is very dense in this material, we could not use the echelle or the compact spectrometer. However, limits of detection for Ag, Ni and Fe were determined using the Czerny–Turner SPEX spectrometer setup (*i.e.* benchtop). These results are presented in Table 2 and also appear to be fairly comparable to those reported in the literature.[40]

Table 2 LIBS limits of detection for Ag, Ni and Fe in a copper matrix with the benchtop spectrometer for two different acquisition methods using the compact fiber laser. Lines used for calculation were normalized by the 353.37 nm Cu line

Spectrometer	Benchtop			
Acquisition method	Single shot		On-chip accumulation	
Element (line)	R^2	LOD/µg g^{-1}	R^2	LOD/µg g^{-1}
Ag (338.29 nm)	0.997	1.9 ± 0.1	0.986	2.4 ± 0.1
Ni (349.30 nm)	0.999	10.4 ± 0.2	0.991	12.9 ± 0.7
Ni (341.48 nm)	0.997	21.3 ± 0.6	0.992	28 ± 1
Fe (358.12 nm)	0.967	13 ± 1	0.989	21 ± 1

4. Conclusions

The interaction between the fiber laser and aluminium solid targets was investigated through crater and plasma characterization and by LIBS performances. Limits of detection in the low µg g^{-1} range have been obtained for Cr, Cu, Fe, Mg, Mn, and Si in aluminium alloys and Ag, Ni, Fe in copper alloys with three different detection systems, including one with a compact spectrometer. This work has demonstrated the fiber laser capabilities for elemental analysis of at least aluminium and copper alloys by LIBS, where analytical performances showed to be, in some cases, close to those obtainable with the traditional high energy Nd:YAG laser. Extension of the possibilities to other materials is also encouraging and currently under investigation in our laboratory.

We found that in some given conditions, the use of a compact spectrometer can allow obtaining low limits of detection and operating at very fast rates, taking more advantage of the high repetition rate feature of the fiber laser. The high repetition rate potential (25 kHz here) is useful for measurements that must be performed rapidly and that require extensive sampling of a surface, to cover a large area or to average over sample inhomogeneities such as in rocks, minerals, powders, *etc.* It can also be very useful for microanalysis or for the detection of inclusions when mapping a large area where a high spatial resolution is needed.

The very high ablation rate of the fiber laser on aluminium targets has been observed both by optical coherence tomography measurements and scanning electron microscopy. The averaged depth per pulse was 7.7 µm in aluminium. The excellent beam quality and the elongated laser pulse—tailing edge up to 200 ns—is proposed as an explanation for this thick depth of ablated mass as both parameters reduce plasma shielding of the laser. For analytical purposes, this ablated depth—in the range of µm pulse^{-1} compared to few nm pulse^{-1} using a traditional ns Nd:YAG laser—offers a unique advantage for LIBS measurements of bulk concentration, since it may be less affected by the thin oxide layer normally formed on the surface of some metals.

Finally, it has been demonstrated that the fiber laser or MOPA technology is already interesting for LIBS applications. However, being a technology which is involved in a wide range of high speed applications, the rapid evolution of the market will push the fiber laser technology to deliver even higher output peak powers. This should open the possibilities even further in a very

near future. Even if the low energy of the fiber lasers is a real limitation for standoff applications, it seems clear that this robust alignment-free technology has a great potential for many industrial LIBS applications, rapid mapping of surfaces or spatially resolved analysis and should therefore be considered as a new laser source alternative.

Acknowledgements

References

1 R. Noll, V. Sturm and M. Stepputat, in *Laser-Induced Breakdown Spectroscopy (LIBS)*, ed. A. W. Miziolek, V. Palleschi and I. Schechter, Cambridge University Press, 2006, pp. 400–439.
2 D. A. Cremers and L. J. Radziemski, *Handbook of Laser-Induced Breakdown Spectroscopy*, Wiley, 2006, pp. 197–226.
3 R. J. Mears, L. Reekie, I. M. Jauncey and D. N. Payne, *Electron. Lett.*, 1987, **23**, 1026–1028.
4 J. A. Alvarez-Chavez, H. L. Offerhaus, J. Nilsson, P. W. Turner, W. A. Clarkson and D. J. Richardson, *Opt. Lett.*, 2000, **25**, 37–39.
5 C. D. Brooks and F. Di Teodoro, *Opt. Express*, 2005, **13**, 8999–9002.
6 F. Di Teodoro and C. D. Brooks, *Opt. Lett.*, 2005, **30**, 3299–3301.
7 J. Limpert, A. Liem, T. Gabler, H. Zellmer, A. Tünnermann, S. Unger, S. Jetschke and H. R. Müller, *Opt. Lett.*, 2001, **26**, 1849–1851.
8 R. Paschotta, J. Nilsson, A. C. Tropper and D. C. Hanna, *IEEE J. Quantum Electron.*, 1997, **33**, 1049–1056.
9 A. Tünnermann, T. Schreiber, F. Röser, A. Liem, S. Höfer, H. Zellmer, S. Nolte and J. Limpert, *J. Phys. B: At., Mol. Opt. Phys.*, 2005, **38**, S681–S693.
10 Y. Wang, *J. Lightwave Technol.*, 2005, **23**, 2139–2147.
11 B. Shiner, *Ind. Laser. Solut. Manuf.*, 2006, **21**, 24–25.
12 A. Freedman, F. J. Iannarilli, Jr and J. C. Wormhoudt, *Spectrochim. Acta, Part B*, 2005, **60**, 1076–1082.
13 C. Lopez-Moreno, K. Amponsah-Manager, B. W. Smith, I. B. Gornushkin, N. Omenetto, S. Palanco, J. J. Laserna and J. D. Winefordner, *J. Anal. At. Spectrom.*, 2005, **20**, 552–556.
14 G. Cristoforetti, S. Legnaioli, V. Palleschi, A. Salvetti, E. Tognoni, P. Alberto Benedetti, F. Brioschi and F. Ferrario, *J. Anal. At. Spectrom.*, 2006, **21**, 697–702.
15 K. Amponsah-Manager, N. Omenetto, B. W. Smith, I. B. Gornushkin and J. D. Winefordner, *J. Anal. At. Spectrom.*, 2005, **20**, 544–551.
16 I. B. Gornushkin, K. Amponsah Manager, B. W. Smith, N. Omenetto and J. D. Winefordner, *Appl. Spectrosc.*, 2004, **58**, 762–769.
17 J. Wormhoudt, F. J. Iannarilli,Jr, S. Jones, K. D. Annen and A. Freedman, *Appl. Spectrosc.*, 2005, **59**, 1098–1102.
18 C. Bohling, D. Scheel, K. Hohmann, W. Schade, M. Reuter and G. Holl, *Appl. Opt.*, 2006, **45**, 3817–3825.
19 M. Baudelet, C. C. C. Willis, L. Shah and M. Richardson, *Opt. Express*, 2010, **18**, 7905–7910.
20 J. Hecht, *Laser Focus World*, 2009, **45**, 53–57.
21 S. Norman and M. Zervas, *Laser Focus World*, 2007, **43**, 93–98.
22 F. Brygo, C. Dutouquet, F. Le Guern, R. Oltra, A. Semerok and J. M. Weulersse, *Appl. Surf. Sci.*, 2006, **252**, 2131–2138.
23 S. M. Klimentov, P. A. Pivovarov, V. I. Konov, D. Breitling and F. Dausinger, *Quantum Electron.*, 2004, **34**, 537–540.
24 K. Y. Yamamoto, D. A. Cremers, L. E. Foster, M. P. Davies and R. D. Harris, *Appl. Spectrosc.*, 2005, **59**, 1082–1097.
25 M. R. H. Knowles, *Opt. Express*, 2000, **7**, 50–55.
26 R. E. Russo, in *Laser-Induced Breakdown Spectroscopy (LIBS)*, ed. A. W. Miziolek, V. Palleschi and I. Schechter, Cambridge University Press, 2006.
27 S.-B. Wen, X. Mao, R. Greif and R. E. Russo, *J. Appl. Phys.*, 2007, **101**, 023114.
28 S.-B. Wen, X. Mao, R. Greif and R. E. Russo, *J. Appl. Phys.*, 2007, **101**, 023115.
29 A. Bogaerts and Z. Chen, *Spectrochim. Acta, Part B*, 2005, **60**, 1280–1307.
30 G. Cristoforetti, G. Lorenzetti, P. A. Benedetti, E. Tognoni, S. Legnaioli and V. Palleschi, *J. Phys. D: Appl. Phys.*, 2009, **42**, 225207.
31 J. F. Y. Gravel and D. Boudreau, *Spectrochim. Acta, Part B*, 2009, **64**, 56–66.
32 M. Sabsabi and P. Cielo, *Appl. Spectrosc.*, 1995, **49**, 499–507.
33 H. Fink, U. Panne and R. Niessner, *Anal. Chem.*, 2002, **74**, 4334–4342.
34 M. Hoehse, D. Mory, S. Florek, F. Weritz, I. Gornushkin and U. Panne, *Spectrochim. Acta, Part B*, 2009, **64**, 1219–1227.
35 T. Kuhlen, C. Fricke-Begemann, N. Strauss and R. Noll, *Spectrochim. Acta, Part B*, 2008, **63**, 1171–1176.
36 M. Sabsabi, V. Detalle, A. Harith Mohamed, W. Tawfik and H. Imam, *Appl. Opt.*, 2003, **42**, 6094–6098.
37 M. A. Ismail, H. Imam, A. Elhassan, W. T. Youniss and M. A. Harith, *J. Anal. At. Spectrom.*, 2004, **19**, 489–494.
38 W. T. Y. Mohamed, *Opt. Laser Technol.*, 2008, **40**, 30–38.
39 T. Sakka, H. Oguchi, S. Masai, K. Hirata, Y. H. Ogata, M. Saeki and H. Ohba, *Appl. Phys. Lett.*, 2006, **88**, 061120.
40 M. Sabsabi and P. Cielo, *J. Anal. At. Spectrom.*, 1995, **10**, 643–647.